

Optical pumping of ultra-relativistic ions

Jacek Bieroń,¹ Mieczysław Witold Krasny,^{2,3} Wiesław Płaczek,¹ and Szymon Pustelný^{4,*}

¹*Institute of Theoretical Physics, Jagiellonian University, Lojasiewicz 11, 30-348 Kraków, Poland*

²*LPNHE, Sorbonne University, CNRS/IN2P3, Tour 33, RdC, 4, pl. Jussieu, 75005 Paris, France*

³*CERN, Esplanade des Particules 1, 1211 Geneva 23, Switzerland*

⁴*M. Smoluchowski Institute of Physics, Jagiellonian University, Lojasiewicz 11, 30-348 Kraków, Poland*

The Gamma Factory (GF) initiative aims at construction of a unique experimental tool exploiting resonant interaction of light with ultra-relativistic partially stripped ions (PSI) stored in circular accelerators at CERN. Resonant excitation of high-energy transitions of the ions is achieved through Doppler-boosting (by twice the Larmor factor; from hundred to several thousand times) of light energy. In order to efficiently excite the ions, and hence generate intense beams of scattered/fluorescent photons, a detailed knowledge of the ions' energy structure and dynamics of optical pumping is required. Spectroscopic properties of PSI selected for the GF operation, as well as their optical pumping schemes are investigated. Two regimes of the light-ion interaction are identified, leading to different dynamics of the pumping process. The efficiency of the light-ion interaction as well as the number of photons emitted from a single ion bunch is estimated, both analytically and numerically, for three ions considered for the GF, i.e. Li-like $^{208}_{82}\text{Pb}^{79+}$, Li-like $^{40}_{20}\text{Ca}^{17+}$, and H-like $^{208}_{82}\text{Pb}^{81+}$.

I. INTRODUCTION

The Gamma Factory (GF) [1] is the first high-energy accelerator-technology-based project for which the precise atomic-physics input is of primordial importance. Firstly, this project requires a high-precision calculations of the atomic energy levels of hydrogen-, helium- and lithium-like partially stripped ions (PSI) to precisely tune the energy of the beams of these ions to resonantly excite their atomic degrees of freedom with Doppler-energy-boosted laser light. Since linewidths of the atomic resonant excitations are much narrower than the excitation frequency, the “resonance-finding” procedure, involving tuning of the ion relativistic Lorentz factor γ_L , will certainly be one of the most difficult operation aspects of the project. Secondly, the lifetimes of the excited states must be calculated to high precision in order to optimize and control the direction, polarization and energy of fluorescence photons.

On top of precise knowledge of the static parameters of the PSI, which will be used in the GF research programme, good understanding of the ion–light interaction dynamics is necessary to optimize parameters of laser pulses as well as to determine spatiotemporal characteristics of ion bunches.

One of the pivotal milestones of the GF project is development of a theoretical framework of interaction of light pulses with ion bunches. In general, the interaction has to be described as the quantum-mechanical process which includes interference of probability amplitudes. In this scope, its probabilistic description, which does not control the quantum superposition of atomic states, is approximate and can only be used in limited context. At the same time, implementation of the process in terms of probabilistic (classical) observables is tempting as it en-

ables application of Monte Carlo generators. The Monte-Carlo framework provides an efficient interface between the theoretical framework and existing software tools, used to describe both the individual particles and collective beam dynamics in high-energy storage rings.

The basic goal of the present paper, being a crucial step for the development of the GF, is to provide a clear assessment under which conditions the probabilistic framework is sufficient and under which conditions it fails. These initial conditions will be specified by the following parameters: (1) the laser-pulse temporal and spatial shape, e.g. its time-dependent energy spectrum and total energy, and (2) the ion-bunch shape and the geometry of interaction.

The paper is organized as follows. In Section II we investigate: the properties of the Li-like Pb ion which may be suitable for the proof-of-principle experiment (PoP) in the Super Proton Synchrotron (SPS) at CERN [2]; the H-like Pb ion which is considered as a candidate for the GF experiment at the LHC [3]; and the He-like Ca and Li-like Ca ions which can be used for radioactive-ion beam production [4] and a high-luminosity option of the LHC with laser-cooled isoscalar ion beams [5], respectively. For the PoP experiment at the SPS, we need an ion which would fit within a three-dimensional window defined as follows: transition energy of $10 - 100 \text{ eV} \times$ lifetime of the excited state of $10 - 100 \text{ ps} \times$ lifetime of the ion beam in the ring. We verified that this condition is fulfilled, both with respect to energy and lifetime, for H-like, He-like, Li-like, Ne-like, Mg-like, Ar-like and Kr-like isoelectronic sequences. We have not investigated Xe-like or Rn-like, nor any other sequence, but it can be done if necessary. In Section III, we discuss optical pumping of PSI in the GF experiments. The calculations are performed for two distinct scenarios: (1) where the Doppler broadening dominates over the natural linewidth of the transition and (2) where two widths are comparable. These lead to two different dynamics of the pumping and emission processes. Finally, Monte Carlo simulation of interactions of a PSI

* Email: pusteln@uj.edu.pl

bunch with a laser-light pulse is described in Section IV. The conclusions are presented in Section V.

II. ENERGIES AND LIFETIMES OF ATOMIC EXCITED LEVELS

Partially stripped ions, which are presently considered as the candidates for the GF are: Li-like Pb, H-like Pb, He-like Ca and Li-like Ca. The energies E_{ik} and lifetimes τ_{ik} for selected transitions in these ions (as well as other candidates mentioned above) were computed with the Dirac–Hartree–Fock package **GRASP** [6–10]. These calculations were made in the Dirac–Hartree–Fock model, i.e. with the Dirac–Coulomb Hamiltonian, with a finite nuclear size modeled as the two-parameter Fermi distribution [11] and with the leading QED corrections (SE and VP) evaluated perturbatively [12]. The electron correlation effects were accounted for through the multiconfiguration variational Complete Active Space approach [13, 14]. The calculated values were compared with other data available in the literature, and in each case the most accurate results were selected in Tables I, II, III, IV, and V.

A. Li-like Pb

The NIST-ASD database [15] lists 46 references on the subject of Pb^{79+} . In Table V, we assumed the lifetime for $2p_{1/2}$ state of Li-like Pb from Johnson, Liu, and Sapirstein [16]. They estimated that their calculated lifetimes are accurate to a fraction of a percent at the neutral end of the isoelectronic sequence, and the accuracy increases at higher Z .

Transition energies for the Li-like Pb ion are collected in Table I. For each calculation we quoted as many digits as provided by the authors. Only the three latest calculations included the estimates of the uncertainty. A comparison with experiment was possible only for the $2s-2p_{3/2}$ line. Eventually, in Table V we assume the $2s-2p_{1/2}$ transition energy $230.823(47)(4)$ eV in Li-like Pb from Yerokhin and Surzhykov [17, 18].

B. H-like Pb

The bibliography of spectroscopic properties of hydrogenic ions lists more than one hundred papers [15, 29]. In the present work we have taken into consideration the papers of Johnson and Soff [26], Beier *et al.* [27], Jitrik and Bunge [28], and Yerokhin and Shabaev [29]. Johnson and Soff [26] have taken into account the QED effects (Lamb shift), the effects of the finite nuclear size, reduced mass, nuclear recoil effects, as well as their respective cross-terms. Beier *et al.* [27] have taken into account the QED effects, the effect of the finite nuclear size, as well as the nuclear recoil effect. Jitrik and

Bunge [28] have evaluated transition energies and rates for hydrogen-like ions using eigenfunctions of the Dirac Hamiltonian with a point nucleus. The discrepancy between the values of Jitrik and Bunge [28] and the values obtained with more elaborate approaches of Johnson and Soff [26], Beier *et al.* [27], and Yerokhin and Shabaev [29] illustrates the contributions of the effects beyond the the Dirac Hamiltonian with a point nucleus. Yerokhin and Shabaev [29] have taken into account the QED effects, the finite nuclear size, the nuclear recoil as well as their respective cross-terms. In particular, they thoroughly evaluated the two-loop QED correction and the finite nuclear size correction, which constitute the dominant sources of uncertainty for the H-like Pb ion. All these authors have assumed different values of the fine structure constant α which were considered standard at the respective publication dates. These differences, ranging between seventh up to tenth figure (the current value of $\alpha^{-1} = 137.035\ 999\ 084(21)$ [30]) contributed to several factors involved in the summation of the transition energy and rate. Eventually, in Table V we assume the energy for the transition $E(1s-2p_{1/2}) = 75280.83(26)$ eV in the H-like Pb ion from Yerokhin and Shabaev [29] and the lifetime (34 attoseconds) calculated in the present work with the Dirac–Coulomb Hamiltonian, with the finite nuclear size and with the leading QED corrections evaluated perturbatively [12].

C. He-like Ca

The calculations of the transition energies and rates for the He-like Ca ion were performed with the **GRASP** package described at the beginning of Section II. The results are presented in Table III and compared with data available in the literature. The transition energy calculated by Artemyev *et al.* [31] is the most reliable among those presented in Table III. For the lifetime one might cautiously assume 6.0(1) ps, i.e. an average of the three values calculated by Lin *et al.* [32], Aggarwal *et al.* [33] and in the present work, respectively.

D. Li-like Ca

Similarly as in the case of He-like Ca, for Li-like Ca ion, the transition energies and lifetimes were calculated using **GRASP** package. The results for four different excitations from the ground state $1s^22s$ are presented in Table IV and compared with data available in the literature.

E. Bright future of partially stripped ions in the Gamma Factory

The Li-like Pb ions will be accelerated and irradiated in the GF PoP experiment at the SPS [2]. During the

TABLE I. Transition energies in the units of eV for the $2s-2p_{1/2}$ and $2s-2p_{3/2}$ lines in the Li-like Pb ion.

$2s-2p_{1/2}$	$2s-2p_{3/2}$	year	method	reference
231.374	2642.297	1990	MCDF VP SE	[19]
230.817	2641.980	1991	MCDF VP SE	[20]
230.698	2641.989	1995	RCI QED NucPol	[21]
231.16	2642.39	1996	3-rd order MBPT	[16]
—	2642.26(10)	2008	expt(EBIT)	[22]
230.68	—	2010	RCI QED NucPol	[23]
230.76(4)	2642.17(4)	2011	S-m. 2-l. NucPol	[24]
230.823(47)(4)	2642.220(46)(4)	2018	RCI QED NucPol	[17, 18]
230.80(5)	2642.20(5)	2019	S-m. 2-l. NucPol	[25]

TABLE II. Transition energies E and lifetimes τ of the $1s-2p_{1/2}$ and $1s-2p_{3/2}$ transitions in the H-like Pb ion.

$1s-2p_{1/2}$		$1s-2p_{3/2}$		reference
E [eV]	τ [as]	E [eV]	τ [as]	
75280.47	—	77934.25	—	[26]
75279	—	—	—	[27]
75521	33.8	78174	38.8	[28]
75280.83(26)	—	77934.59(27)	—	[29]
75278	34.1	77935	39.2	this work

TABLE III. Transition energy E and lifetime τ of the $1s^2-1s2p\ ^1P_1$ transitions in the He-like Ca ion.

E [eV]	τ [ps]	reference
—	6.06	[32]
3902.3676	—	[34]
3902.3775(4)	—	[31]
3902.2570	5.946	[33]
3902.2551	—	[15]
3902.3351	6.09	this work

experiment, various aspect of the project, including efficiency of the PSI excitation, will be studied. This will be the next step in the project which may open means for the GF implementation at the Large Hadron Collider (LHC). For that experiment, the H-like Pb ion with much larger transition energy is considered [3]. The transition becomes accessible for existing light sources, such as the Free Electron Laser (FEL), in conjunction with a higher value of the Lorentz factor γ_L of the PSI bunches. The He-like Ca ions can be also used for the radioactive-ion beam production at the GF [4], while the Li-like Ca ions are suggested for the high-luminosity version of the LHC with laser-cooled isoscalar ion beams [5]. In the following section we analyze the interaction of the laser light with the PSI bunch circulating in these two accelerators, investigating different scenarios of the process.

III. OPTICAL PUMPING OF IONS

In high-energy physics, a scattering cross section is often used to describe a scattering process. While in optics the cross section is also used, it is noteworthy that its application implicitly assumes that the process is investigated under the steady state, when dynamic equilibrium between different processes (e.g. excitation and relaxation) is being reached. However, prior to the steady state, an illuminated system experiences a transient period during which it undergoes dynamic changes. The dynamics of this transient evolution depends on many parameters, including incident-light intensity, strength of an atomic transition, light detuning or excited-state relaxation. Thereby, over time comparable with the excited-state lifetime τ_e the population of the state, determining fluorescence intensity, may continuously increase, eventually reaching its steady-state value, but it may also experience strong oscillations before finally leveling up at a specific value. As the frequency and amplitude of these, so-called, Rabi oscillations depend on parameters of incident light, studies of the excitation of PSI in a bunch, experiencing strong inhomogeneous (Doppler) broadening of the transition, $\Delta\omega/\omega_0 \approx 10^{-4}$, where ω_0 is the transition frequency and $\Delta\omega$ is its broadening, with pulsed light of a temporal length comparable to the excited-state lifetime becomes an important aspect of the GF.

Below, we analyze theoretically and numerically the problem of optical pumping of an energy-dispersed ion bunch by pulsed light. By investigating interaction of a resonant light pulse with a generic closed two-level system, i.e. with other levels ignored, we analyze the situation which, to the first order, reproduces the GF set-up.

A. Theoretical model

We consider an excitation of a two-level atom with semi-resonant light, $\Delta\omega \ll \omega$, where ω is the light frequency and $\Delta\omega$ is its detuning from the optical transi-

TABLE IV. Transition energies E and lifetimes τ of the 2s–2p_{1/2}, 2s–2p_{3/2}, 2s–3p_{1/2}, 2s–3p_{3/2} transitions in the Li-like Ca ion.

2s–2p _{1/2}		2s–2p _{3/2}		2s–3p _{1/2}		2s–3p _{3/2}		ref.
E [eV]	τ [ns]	E [eV]	τ [ns]	E [eV]	τ [ps]	E [eV]	τ [ps]	
35.9625		41.0286		661.8896		663.3403		[15]
35.959	0.767	41.027	0.512	661.776	0.428	663.278	0.436	this work
35.963	0.7680	41.029	0.5123					[16]
35.96119(73)		41.02497(78)						[18]
35.962(1)		41.024(1)						[35]
				661.7643	0.4282	663.2660	0.4367	[36]
				663	0.4167	663	0.4274	[37]
0.76752		0.51258						[38]
experiment								
35.962(2)								[39]
		41.029(2)						[40]

tion. Since the two-level system is considered, there are no dark states, which could trap atoms, preventing from its successive excitation. In this system, the atoms are characterized with the excited-state relaxation rate γ_e , and we also assume that the atoms live infinitely long in the ground state, $\gamma_g = 0$. Finally, the interaction is considered in the rotating-wave approximation, i.e. the interaction with only a resonant component of the light field ($\omega \approx \omega_0$) is considered, while the effect of the second frequency component, $-\omega$, is neglected.

In order to determine scattering of photons by the atoms, the time-dependent expectation value of the spontaneous-emission operator \mathcal{F} needs to be calculated [41]

$$\langle \mathcal{F} \rangle = \text{Tr}(\rho \mathcal{F}), \quad (1)$$

where ρ is the density matrix of the atoms. Evolution of the density matrix can be described using the Liouville equation

$$\dot{\rho} = \frac{i}{\hbar} [H, \rho] - \frac{1}{2} \{ \Gamma, \rho \}, \quad (2)$$

where H is the Hamiltonian of the system, containing the contribution from the Hamiltonian of the unperturbed atoms H_0 and the operator V describing their interaction with light. The operator Γ describes relaxation in the system, in particular the relaxation of the excited state due to spontaneous emission. It can be shown [41] that, in the case of a two-level system, the matrix elements of the fluorescence operator are given by

$$F_g^e = \frac{4}{3} \frac{\omega_0^3}{\hbar c^3} \vec{d}_{ge} \cdot \vec{d}_{eg}, \quad (3)$$

where \vec{d}_{eg} is the electric dipole moment between the g and e states. Because the electric dipole moment is an odd operator, the only nonzero elements of the fluorescence

operator \mathcal{F} are at a diagonal. Moreover, since the fluorescence arises exclusively due to spontaneous emission, and the ground state is relaxation free, the fluorescence of the atoms is proportional to the excited-state population ρ_{ee}

$$\langle \mathcal{F} \rangle = \frac{3\gamma_e N_{\text{PSI}}}{\hbar c^3} \rho_{ee}, \quad (4)$$

where N_{PSI} is the number of the partially stripped ions.

Since the only dynamic parameter in Equation 4 is the excited-state population ρ_{ee} , henceforth we investigate evolution of the population. Moreover, normalization of the population, i.e. $\rho_{gg} + \rho_{ee} = 1$, where ρ_{gg} is the ground-state population, allows to relate the population ρ_{ee} with the probability of the excited-state occupation, also providing an intuitive understanding of the efficiency of pumping of PSI and their successive fluorescence.

The problem of the interaction of the classical light with the two-level atom using the Liouville equation is considered in many textbooks (see, e.g. [41]):

$$\dot{\rho}_{eg} = i \left(\Delta\omega + \frac{i\gamma_e}{2} \right) \rho_{eg} - \frac{i\Omega_R}{2} (\rho_{gg} - \rho_{ee}), \quad (5)$$

$$\dot{\rho}_{ge} = -i \left(\Delta\omega - \frac{i\gamma_e}{2} \right) \rho_{ge} + \frac{i\Omega_R}{2} (\rho_{gg} - \rho_{ee}), \quad (6)$$

$$\dot{\rho}_{ee} = \frac{i\Omega_R}{2} (\rho_{ge} - \rho_{eg}) - \gamma_e \rho_{ee}, \quad (7)$$

where ρ_{eg} is the optical coherence (an amplitude of the superposition of the g and e states) and

$$\Omega_R = c \sqrt{\frac{6\pi\gamma_e I}{\hbar\omega_0^3}} \quad (8)$$

is the Rabi frequency characterizing the coupling strength between the light and the ions, and I is light

intensity. Solving this set of equation allows one to determine the excited state population, and hence the light scattering.

B. Scattering at steady state

Let us first consider the stationary situation when balance between various processes is achieved, i.e. the steady-state situation. Under such a regime, the left-hand sides of Equations 5–7 are equal to zero, $\dot{\rho} = 0$, which allows us to calculate the excited-state population

$$\rho_{ee} = \frac{\Omega_R^2/4}{\Delta\tilde{\omega}^2 + \gamma_e^2/4 + \Omega_R^2/2} = \frac{\kappa_1/2}{1 + 4\Delta\tilde{\omega}^2 + \kappa_1}, \quad (9)$$

where $\Delta\tilde{\omega} = \Delta\omega/\gamma_e$ is the normalized detuning and $\kappa_1 = 2\Omega_R^2/\gamma_e^2$ is the saturation parameter characterizing the strength of the light-atom coupling with respect to the system's relaxation γ_e . In particular, Equation 9 shows that the excited-state population, and hence fluorescence, depends on the light intensity and detuning.

Comparison of Equation 9 with the classical absorption cross section, determining the efficiency of light scattering [42],

$$\sigma = \frac{\sigma_0}{1 + 4\Delta\omega^2/\gamma_e^2 + 2\Omega_R^2/\gamma_e^2} = \frac{\sigma_0}{1 + 4\Delta\omega^2/\gamma_t^2}, \quad (10)$$

where σ_0 is the resonant absorption cross section and γ_t is the transition linewidth, reveals similarity between the classical and quantum approach. In particular, both approaches show that the further the light is detuned from the optical transition, the less efficient the excitation is. Both the classical and the quantum-mechanical approach also reveal the dependence of the scattering on the transition linewidth. In the classical approach, this is the light-intensity independent width γ_t , which in the low-intensity regime would correspond to the excited-state relaxation rate γ_e , i.e. $\gamma_t = \gamma_e$. However, the comparison also reveals that the quantum-mechanical approach also incorporates the saturation effect which modifies the transition width. This would manifest in the classical approach as broadening of the linewidth due to the light intensity, $\gamma_t = f(I)$. The saturation effect stems from the finite number of atoms that can scatter light and the finite lifetime of the excited state τ_e . In turn, at some point the further increase of the incident light intensity does not result in the increase of the number of absorbed/scattered photons. In fact, it can be shown that under the steady state, the total number of atoms that may be introduced into the excited state is a half of the total population (note that this is not the case of the coherent evolution described in the subsequent section). This is a result of stimulated emission, according to which if more atoms are present in the excited state, the incident light, instead of further exciting the ions, induces their deexcitation and emission of photons indistinguishable from the incident ones. Finally, Equation 9 shows

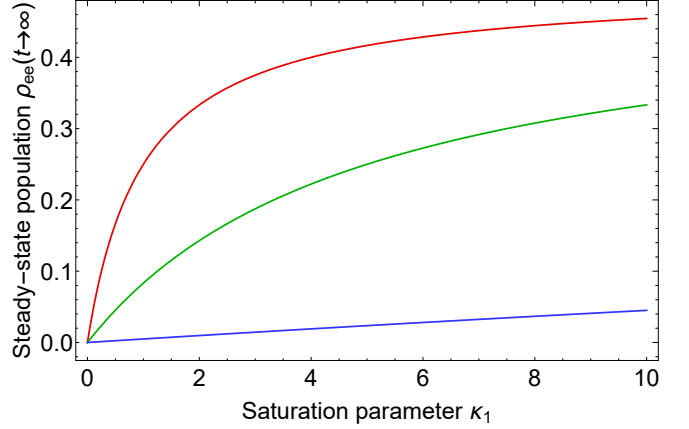


FIG. 1. The steady-state excited-state population ρ_{ee} , determining the fluorescence of the PSI illuminated with light, versus the saturation parameter κ_1 for three different normalized detunings: $\Delta\tilde{\omega} = 0$ (red), $\Delta\tilde{\omega} = 1$ (green) and $\Delta\tilde{\omega} = -5$ (blue).

that saturating the transition for off-resonance beams requires more intense incident light than in the resonant case.

The discussion presented above is depicted with the quantum-mechanical results shown in Figure 1, where the excited-state population is plotted against the saturation parameter κ_1 for three different detunings. As expected, increasing the light power (saturation parameters) improves the excited-state population and hence the intensity of the scattered light. While initially the process linearly depends on incident-light intensity, at higher intensity it begins to saturate. The results also show that saturating the transition with the detuned light requires a more intense incident light. This dependence also indicates that saturating moving ions, whose transition frequencies in the laboratory (LAB) frame are modified due to the Doppler effect, using a CW light, is more challenging.

The remaining question is how fast the system reaches the steady state, which can be rephrased into: when the classical approach adequately describes the atom–light interaction (even if we include the transition broadening due to the light, i.e. when the κ_1 effect is taken into account). From the analysis of Equations 5–7 one can show that the system reaches its steady state within times comparable to the excited-state lifetime τ_e . This indicates a fundamental role of the spontaneous emission. If the interaction time is shorter than τ_e , the classical approach using the cross section does not work and dynamics of the system needs to be evaluated using the quantum-mechanical formalism. This evolution is discussed in the following section.

C. Dynamics of optical pumping

The ultrarelativistic nature of the ions results in significant difference in the flow of time in the ion-rest and LAB frames. As a result, the excited-state lifetime in the ion-rest frame (IRF) τ_e corresponds to the LAB-frame excitation time τ_e^{LAB} via

$$\tau_e^{\text{LAB}} = \gamma_L \tau_e. \quad (11)$$

As a consequence, the average path an excited ion propagates in the LAB frame is

$$l^{\text{LAB}} = c \gamma_L \tau_e. \quad (12)$$

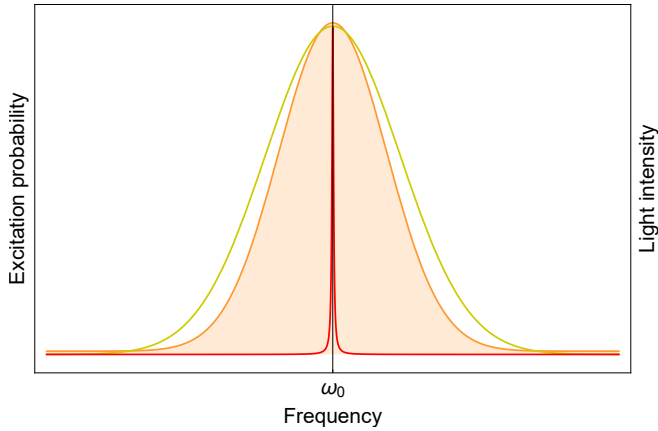


FIG. 2. Schematics of spectral characteristics of the system. Red line shows the probability of excitation of the motionless PSI. In a weak-light regime, the probability is given by the Lorentz function whose half-width at the half-maximum is determined by the excited-state relaxation rate γ_e . The middle orange line corresponds to the spectral profile of the pulse used for the excitation, where shading indicates the frequency range that can be used for the ion excitation. The broadest profile corresponds to the transition line inhomogeneously broadened due to the Doppler effect.

The ions intended to be used in the GF will be excited at a relatively narrow transition, $\omega_0 \gg \gamma_e$. However, due to the ion energy dispersion $\Delta\mathcal{E}/\mathcal{E} = \Delta\gamma_L/\gamma_L$, the transition is inhomogeneously broadened (the Doppler effect). In the PoP experiment [2], the Doppler broadening Γ_D of the transition is 2–4 orders of magnitude larger than its natural width γ_e , as schematically depicted in Figure 2. Conventionally, this would imply a necessity of application of a much stronger light to saturate the transition and efficiently populate the excited state, cf. Equation 9. However, even under such conditions, the PSI moving with different velocities have different detunings, and hence are differently saturated. In turn, this degrades the efficiency of optical pumping. Additional complication is that, in the GF, the PSI interact with the light just for a finite time. Thereby, instead of interacting with the CW light, they experience the spectrally

broadened light. In fact, we exploit this effect to facilitate the interaction and more efficiently pump the atoms. This is achieved by generating light whose ion-rest-frame spectral width coincides with the Doppler width of the ion bunch

$$t_p^{\text{LAB}} = \gamma_L/\Gamma_D. \quad (13)$$

The spectral broadening of the pulse well beyond the transition natural linewidth has important consequences. It allows to neglect the relaxation of the ions during the optical pumping, which significantly simplifies the theoretical description. In fact, the interaction of the light with the relaxation-free two-level atom is a textbook example (see, e.g. [43]), demonstrating oscillations of the excited-state population $\rho_{ee}(t)$ at the Rabi frequency Ω_R (the Rabi oscillations). While dynamics of this coherent, i.e. uninterrupted by dephasing spontaneous emission, evolution is harder to be determined in the case of pulsed excitation, where the Rabi frequency varies over time, we can generally state that the excited-state population at the time moment t_1 is given by $\sin\left(\int_0^{t_1} \Omega_R(t)dt\right)$, where the Rabi frequency $\Omega_R(t)$ is time dependent.

From the perspective of the GF, the last consequence of the short length of the pulse is the absence of ion–ion interactions (e.g. collisions) during the optical pumping. As the PSI in different velocity classes can be treated independently, the problem can be further simplified and the excited-state population of the whole bunch is simply a weighted average over the ions' velocity distribution.

The final step in our discussion concerns the efficiency of the excitation of atoms with different detunings. In the case of the interaction with the pulse spectrally coinciding with the Doppler width, the different velocity classes are resonantly excited by appropriate spectral components of the light. This alleviates the demanding requirement for the light intensity, which may lead to the problems with photoionization or multiphoton excitation. Moreover, this also provides a better control over the efficiency of the pumping. As shown in Figure 3, the interaction with such a pulse, whose central frequency ω is detuned from the resonance by the Doppler width, $\Delta\omega = \Gamma_D$, reduces the excitation efficiency by a half. In the case of the spectrally narrow light, this case would correspond to zero excitations, unless the extremely strong light is used.

Under the assumption of a short light pulse, the efficiency of the pumping of the whole PSI bunch can be calculated by averaging over the distribution due to the energy dispersion. In the optimal case, i.e. when the pulse amplitude is chosen in such a way that in-resonance ions experience a half of the Rabi cycle, i.e. have been completely transferred into the excited state, and the pulse width coincides with the ions Doppler broadening, $\gamma_p^{\text{IRF}} = \Gamma_D$, the efficiency of a whole bunch pumping reaches 70%. Thereby, the PSI can be efficiently pumped.

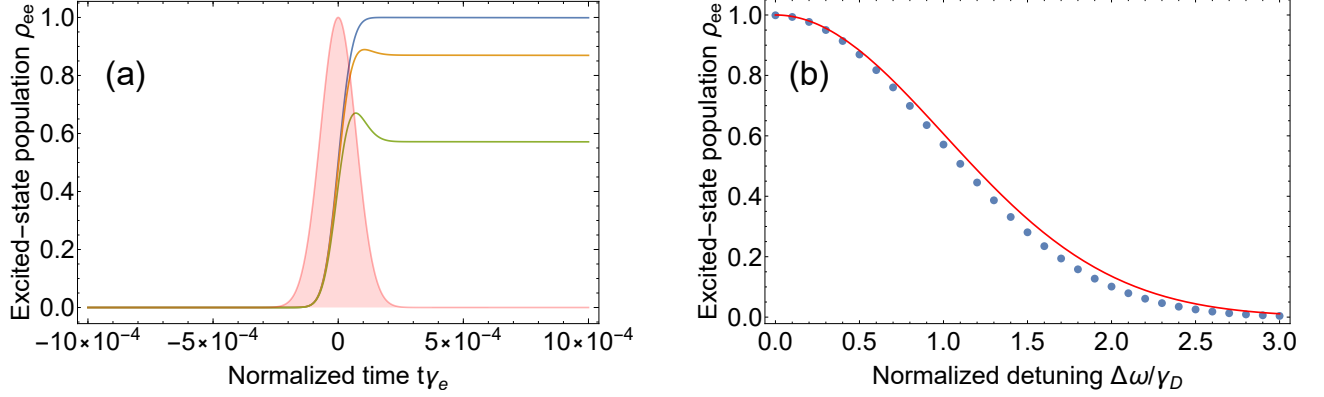


FIG. 3. (a) The excited-state population of the PSI interacting with the Gaussian light pulse (red trace) of a spectral width coinciding with the atoms' Doppler profile, $\gamma_p^{\text{IRF}} = \gamma_D$. Different traces corresponds to different detunings of the light central frequency ω from the Doppler-shifted resonance frequency: $\Delta\omega/\gamma_D = 0$ (blue), $\Delta\omega/\gamma_D = 0.5$ (yellow), and $\Delta\omega/\gamma_D = 1$ (green). (b) The population of the excited states after the pulse (blue dots) along with the number of the PSI in a specific velocity class (red line) versus the normalized detuning. The results indicate that the PSI-distribution averaged population of the excited state is 70%. The simulations were performed for the pulse spectrally covering the whole inhomogeneously broadened spectral line and the amplitude of the pulse $\Omega_R^0 \approx 18000 \gamma_e$.

D. Optical parameters in real experiment

Let us finally discuss the optical pumping of the PSI in three scenarios considered for the GF: the Li-like lead, planned to be used in the PoP experiment in the SPS [2], the H-like Pb envisioned for the LHC experiment [44] and the Li-like Ca for the case of optical cooling of accelerator beams [5]. Table V summarizes the parameters based on the literature data and the results of calculations performed in this work.

In the PoP experiment in SPS, the lithium-like lead ion ($^{208}_{82}\text{Pb}^{79+}$) will be used. With the Lorentz factor $\gamma_L = 96.3$ and an excitation frequency between the two lowest electronic levels of ~ 230 eV, one can show that the transition can be induced with a Ti:sapphire laser, emitting the infra-red radiation at 1035 nm. Since the inhomogeneous Doppler broadening of the transition is several orders of magnitude larger than the natural linewidth of the transition, to maximize the optical-pumping efficiency, the pulse length is chosen in such a way that it spectrally covers the whole Doppler-broadened spectrum of the PSI bunch. This implies that the pumping is performed in a dynamic regime, where Rabi oscillations are observed, cf. Section. III C. Under such conditions, the energy of the pulse needs to be chosen in such a way that the cumulative phase of the in-resonance Rabi oscillation is equal to π i.e. the PSI are coherently transferred to the excited state. This may be achieved by the pulse energy of $850 \mu\text{J}$, which corresponds to the IRF Rabi-frequency amplitude of the pulse of $7.8 \times 10^{14} \text{ s}^{-1}$. Under such conditions, nearly 55% of all the ions are transferred to the excited state, which will allow to generate up to 4.9×10^7 photons from each PSI bunch. The photons will be emitted within several nanoseconds over a distance of a few meters.

A similar situation is encountered in the case of the lithium-like calcium ion ($^{40}_{20}\text{Ca}^{17+}$). Also in this case, the Doppler-broadened transition is several orders of magnitude larger than its natural linewidth, however, the difference is smaller than in the previous case. This manifests via a larger contribution of the relaxation to the process. The transition may be induced with the light pulse of the carrier wavelength of 771 nm, the pulse length of 2.0 ps, and the pulse energy of $60 \mu\text{J}$. Since the spectral width of the pulse is a half of the Doppler width of the transition, the optical pumping is not as efficient as in the previous case and about 40% of the ions can be excited under such optimized conditions. This corresponds to about 1.4×10^9 photons emitted from each PSI bunch within about 10 ps at the distance of 3 cm.

A completely different situation is encountered in the case of the hydrogen-like lead ion ($^{209}_{82}\text{Pb}^{81+}$). As shown in Table V, the natural linewidth of the transition is slightly larger than the Doppler-broadening due to energy dispersion. Thus, it can be assumed that even with a spectrally narrow pulse all the ions are pumped with comparable efficiency. Specifically, the efficiency drops by a factor of 2 for the detuning γ_e . Another important difference is the light-induced evolution of the excited-state population, determining the fluorescence of the ions. In contrast to the previous cases, the pulse is orders of magnitude longer than the excited-state lifetime, thus the system reaches the equilibrium during each instant of the optical pulse. Thereby, the classical cross-section approach can be used in the considered case. Moreover, the difference in the excited-state lifetime and pulse length suggests that during the light pulse each ion undergoes up to several thousands of pumping-emission cycles. This significantly enhances the photon emission from the ions, even though the efficiency of the excitation is low. The

TABLE V. The optical parameters for the planned GF experiments. The relative energy spread of 2×10^{-4} for both the PSI bunch and the laser pulse is assumed in all cases.

Parameter name	Li-like $^{208}_{82}\text{Pb}^{79+}$	Li-like $^{40}_{20}\text{Ca}^{17+}$	H-like $^{208}_{82}\text{Pb}^{81+}$
Electronic transition	$2s \rightarrow 2p_{1/2}$	$2s \rightarrow 3p_{1/2}$	$1s \rightarrow 2p_{1/2}$
Transition energy ω_0 [eV]	230.823 (47)(4) [17, 18]	661.89 [15]	75 280.83 (26) [29]
Excited-state lifetime τ_e [ps]	76.6 [16]	0.43 ^(a)	3.4×10^{-5} ^(a)
Excited-state relaxation rate γ_e [s $^{-1}$]	1.30×10^{10}	2.3×10^{12}	3.0×10^{16}
Doppler width Γ_D [s $^{-1}$]	7.0×10^{13}	2.0×10^{14}	2.3×10^{16}
Pulse energy [mJ]	0.85	0.06	5.0 ^(b)
LAB-frame radiation frequency [eV]	1.2	1.6	12.6
LAB-frame pulse length τ_p^{LAB} [ps]	1.4	2.0	500
R.M.S. transverse pulse size at focus $\sigma_x = \sigma_y$ [m]	6.5×10^{-4}	5.6×10^{-4}	2.5×10^{-5}
Number of ions per bunch N_b	9×10^7	4×10^9	9.4×10^7
Lorentz relativistic factor of ion γ_L	96.3	205.62	2989
R.M.S. transverse ion beam size [m]	$\sigma_x = 10.5 \times 10^{-4}$ $\sigma_y = 8.3 \times 10^{-4}$ 0.06386	$\sigma_x = 8.0 \times 10^{-4}$ $\sigma_y = 5.7 \times 10^{-4}$ 0.10	$\sigma_x = 3.9 \times 10^{-5}$ $\sigma_y = 3.9 \times 10^{-5}$ 0.15
R.M.S. ion bunch length σ_z [m]			
R.M.S. IRF pulse spectral width γ_p^{IRF} [s $^{-1}$]	6.9×10^{13}	1.0×10^{14}	6.0×10^{12}
IRF pulse amplitude Ω_0^{IRF} [s $^{-1}$]	7.8×10^{13}	1.3×10^{14}	4.3×10^{16}
Characteristic distance after excitation x^{LAB} [m]	2.2	0.027	3×10^{-5}
Estimated number of photons emitted from the bunch	4.9×10^7	1.4×10^9	1.2×10^9

^(a) This work.

^(b) Power inaccessible for the current light sources at wavelengths ~ 100 nm, but anticipated in the future.

rough estimates of the pumping indicates that roughly 1.2×10^9 photons can be emitted from each bunch with the excitation-pulse energy of 5 mJ, which is not yet accessible experimentally, but is foreseen in the future. This result indicates that on average each PSI scatters multiply photons. This can be increased further (up to a factor of about 100), if a more intense light is used.

Up to this point, all the estimations have been performed in a simplified scenario neglecting various effects. Particularly, the spatiotemporal (Gaussian) profile of the light pulse as well as the geometric and momentum distributions of the PSI in the bunch were ignored. These factors, however, may have an effect on the efficiency of the optical pumping and hence the intensity of the scattered light (secondary photons). To take the effects into account, below we present results of numerical simulations of hydrogen-like lead ions ($^{208}_{82}\text{Pb}^{81+}$) using the classical cross section, well motivated in the case, which accommodate for the spatial and temporal profile of the light beam and the PSI bunch.

IV. SIMULATIONS OF OPTICAL PUMPING

As discussed in Subsection III B, in the steady-state and low-intensity regime, the calculations of the ion-light interactions may be performed using the classical cross section. In particular, numerical simulations of the interaction in the GF can be performed in a similar manner as for light sources based on the inverse Compton scat-

tering [45]. In such a case, one only needs to replace the Compton-scattering cross section with the absorption cross section given by Equation 10. We implement this approach using GF-CAIN [46], a Monte Carlo event generator, being a customized (GF-adapted) version of the simulation code CAIN [47] developed by K. Yokoya *et al.* at KEK-Tsukuba, Japan, for the ILC project [48].

The PSI bunch is characterized in terms of standard high-energy particle beam parameters, such as emittances, beta-functions, etc., while the laser pulse is described by a space-time profile function, e.g. the Gaussian distribution. Since the number of particles in a bunch can be huge, making the simulation of interactions of each individual particle with laser-photons unfeasible due to CPU-time and computer memory limitations, one usually replaces some number of physical particles by the, so-called, macroparticle and performs the actual simulations for a lower number of such macroparticles. Then, to each macroparticle one assigns a Monte Carlo weight, which is equal to the number of physical particles it represents. Of course, the smaller the weight the better, because then the simulations are more precise in terms of systematic effects.

The simulations proceed in such a way that at the beginning the bunch of macroparticles and a laser pulse are put some distance away in the z -direction in the LAB frame, and then as time progresses they pass through each other in discrete time steps. In each time step, the macroparticles interact with laser photons according to a given probability and, if excited, secondary photons are

emitted from them through spontaneous emission. After a predefined number of steps the simulation is finished. Then, the outgoing particles can be transformed without interactions to a given value of the z -coordinate or the time-coordinate. In this final position, the space-time coordinates and four-momenta of all outgoing particles are recorded.

The basic quantity used in the simulation of the interaction of a single macroparticle m ($m = 1, \dots, M$), being in the spatial position \vec{r} and having the momentum \vec{p} in the LAB frame, with laser photons is the scattering probability during a time step $\Delta t_i = t_i - t_{i-1}$, where t_i is the time of the i -th step, which is defined as

$$P_m(\vec{r}, \vec{p}, \vec{k}, t_i) = \sigma_{\text{abs}}(\vec{p}, \vec{k}) \left(1 - \vec{\beta} \cdot \vec{k} / |\vec{k}|\right) n_p(\vec{r}, \vec{k}, t_i) c \Delta t_i. \quad (14)$$

where \vec{k} is the light wave vector, \vec{p} and $\vec{\beta}$ are the PSI momentum and relativistic velocity, respectively, $n_p(\vec{r}, \vec{k}, t_i)$ is the local density of the photons, and $\sigma_{\text{abs}}(\vec{p}, \vec{k})$ is the absorption cross section given by [3]

$$\sigma_{\text{abs}}(\vec{p}, \vec{k}) = \frac{\pi r_e c f \gamma_e}{[\gamma_L \omega^{\text{LAB}} (1 - \beta \cos \psi) - \omega_0]^2 + \gamma_e^2 / 4}, \quad (15)$$

where r_e is the classical electron radius, f is the oscillator strength, ω^{LAB} is the irradiated light frequency in the LAB frame, and ψ is the angle between the directions of the light and PSI propagation in this frame.

The above can also be expressed in the following way

$$\sigma_{\text{abs}}(\vec{p}, \vec{k}) = \frac{\sigma_0}{1 + 4\tau_e^2 \Delta\omega^2}, \quad (16)$$

where

$$\sigma_0 = \frac{\lambda_0^2 g_e}{2\pi g_g}, \quad (17)$$

with $\tau_e = 1/\gamma_e$ being the mean lifetime of the excited state, g_g and g_e being the degeneracy factors of the ground state g and the excited state e , respectively, detuning $\Delta\omega = \omega - \omega_0$ measured in the IRF, where the IRF light frequency is given by $\omega = \gamma_L (1 - \beta \cos \psi) \omega^{\text{LAB}}$, and λ_0 being the light central wavelength in the IRF.

For P_m to act as probability, the size of the time step Δt_i in Equation 14 must be adjusted such that

$$0 \leq P_m(\vec{r}, \vec{p}, \vec{k}, t_i) \leq 1, \quad \forall m=1, \dots, M. \quad (18)$$

In the simulations, the step size is set in such a way that if, for some macroparticle m and time t_i , P_m is larger than 1, the corresponding Δt_i is divided into smaller steps until the condition given by Equation 18 is fulfilled.

After computing the probability $P_m^i \equiv P_m(\vec{r}, \vec{p}, \vec{k}, t_i)$, a scattering event is sampled using the (von Neumann) acceptance-rejection Monte Carlo method, see e.g. [49],

$$\{0, 1\} \ni n_m^i = \int_0^1 dR \Theta(P_m^i - R), \quad (19)$$

where Θ is the step function, i.e. a random number R from the uniform distribution on $(0, 1)$ is generated, and if $R \leq P_m^i$, the event is accepted, otherwise it is rejected. If the event is accepted, the corresponding macroparticle is marked as *excited*, which corresponds to the excitation of the PSI. The macroparticle “lives” in the excited state for a time τ which is generated from the exponential distribution

$$\zeta(\tau) = \frac{1}{\tau_e} e^{-\tau/\tau_e}, \quad \tau \geq 0. \quad (20)$$

While in the excited state, the macroparticle can interact with a laser photon and be deexcited by stimulated emission with the probability

$$S_m(\vec{r}, \vec{p}, \vec{k}, t_i) = \frac{g_g}{g_e} P_m(\vec{r}, \vec{p}, \vec{k}, t_i). \quad (21)$$

The stimulated emission event is generated, similarly as above, with the acceptance-rejection Monte Carlo method

$$\{0, 1\} \ni k_m^i = \int_0^1 dR \Theta(S_m^i - R), \quad (22)$$

where $S_m^i \equiv S_m(\vec{r}, \vec{p}, \vec{k}, t_i)$. The corresponding emitted photon is not stored in the event record as it goes along the laser pulse.

If the excited ion is not deexcited by the stimulated emission within its lifetime τ , it undergoes the spontaneous emission. In such a case, the frequency ω_1 as well as the polar θ_1 and azimuthal ϕ_1 angles of the emitted photon are generated in the ion reference frame (IRF), and then they are Lorentz-transformed to the LAB frame. The photon frequency is generated from the Lorentzian distribution, as given in Equation 16, while the emission angles are generated according to the angular distribution of fluorescence corresponding to a given atomic transition. For such a photon, its LAB-frame four-momentum and space-time coordinates of the spontaneous emission are stored in the event record.

After the stimulated or spontaneous emission, the ion returns to its atomic ground state and is ready for absorption of another photon. The whole above procedure is repeated for each macroparticle $m = 1, \dots, M$ at a given time t_i and is done for all time steps $\Delta t_i, i = 1, \dots, I$. The number of the spontaneously emitted photons from the PSI bunch is

$$N_\gamma = \sum_{i=1}^I \sum_{m=1}^M (n_m^i - k_m^i) \frac{N_b}{M}, \quad (23)$$

where N_b is the number of the PSI in the bunch, and N_b/M is the Monte Carlo weight assigned to each macroparticle in the event record.

In a real experiment, the ions in the bunch and the photons in the laser pulse are not monoenergetic, but have some finite energy spread. In the original CAIN program the relative energy spread of particles in a bunch

can be set in the input parameters and then the individual particle energy, i.e. the PSI Lorentz factor γ_L in Equation 15, is generated from an appropriate Gaussian distribution. On the other hand, the laser pulse is assumed to be monochromatic. For the inverse Compton scattering this is not important because the cross section does not depend strongly on the photon energy, but for the resonant absorption the finite energy spread of the laser pulse must be taken into account, particularly for the small linewidth γ_e (cf. Equation 15). It can be generated in the LAB frame from the Gaussian distribution

$$\mathcal{D}(\omega^{\text{LAB}}) = \frac{1}{\sqrt{2\pi} \sigma_{\omega^{\text{LAB}}}} \exp \left[-\frac{(\omega^{\text{LAB}} - \omega_0^{\text{LAB}})^2}{2\sigma_{\omega^{\text{LAB}}}^2} \right] \quad (24)$$

for a given relative frequency spread r.m.s. of a laser pulse $\sigma_{\omega^{\text{LAB}}} / \omega_0^{\text{LAB}}$, where ω_0^{LAB} is the central value of the laser-photon pulse frequency, adjusted to the central value of the absorption resonance for the central value of the PSI-bunch energy spread.

However, Monte Carlo simulations with the above method of the laser-photon energy spread can be inefficient for very narrow resonances, i.e. $\gamma_e \ll \sigma_{\omega}$, where σ_{ω} is the photon frequency width in IRF, because in such a case most of the generated photon frequencies would be off-resonance. In GF-GAIN this method of photon-energy spread generation is applied only when $2\sigma_{\omega}/\omega_0 < \gamma_e/\omega_0$. Otherwise, the photon frequency ω in IRF is generated from the Lorentzian distribution of Equation 16 and the absorption cross section $\sigma_{\text{abs}}(\vec{p}, \vec{k})$ in Equation 14 is replaced with the “spread” cross section

$$\sigma_{\text{spr}}(\vec{p}, \vec{k}) = \sigma_0 \frac{\sqrt{\pi} \gamma_e}{2\sqrt{2} \sigma_{\omega}} \exp \left[-\frac{(\omega - \omega_0)^2}{2\sigma_{\omega}^2} \right], \quad (25)$$

where $\sigma_{\omega}/\omega_0 = \sigma_{\omega^{\text{LAB}}}/\omega_0^{\text{LAB}}$ and σ_0 is given in Equation 17.

In this way, the Monte Carlo simulations are efficient for arbitrary values of the resonance linewidth γ_e and the laser-photon frequency spread r.m.s. $\sigma_{\omega^{\text{LAB}}}$. GF-CAIN has been cross-checked with the independent Monte Carlo generators GF-CMCC and GF-Python, and a good agreement with these programs has been found [2, 50].

As discussed in the previous section, the above description can be applied reliably only for the H-like lead case of the GF presented in the third column of Table V. Below we show some numerical results of the Monte Carlo simulations performed with GF-CAIN for the input parameters given in the third column of Table V, with the supplementary parameters collected in Table VI. The number of the spontaneously emitted photons from the PSI bunch is provided in the last row of Table VI – it corresponds to the emission rate of ~ 2.5 of photons per ion. It agrees up a factor of 5 with the result of the semi-analytical calculations presented in the third column of Table V – the difference being a result of approximations used in the latter, as discussed in the previous section. We have also checked that the emission rate grows linearly with the pulse energy between 0.05 and 5 mJ.

The energy and emission-angle distributions of the outgoing photons are presented in Figures 4 and 5. As can be seen in the left panel of Figure 4, the energy distribution of emitted photons is flat in the range from 0 to $E_{\gamma}^{\text{max}} \approx 450$ MeV. This results from the fact that for this atomic transition the angular distribution of spontaneous emission is uniform in the PSI reference frame. The right panel of Figure 4 shows that the emitted photons are strongly collimated – most of them are emitted within the angle of 1 mrad, with the maximum at ~ 0.25 mrad.

The left panel of Figure 5 shows strong correlations between the energy and angle of the emitted photons. Specifically, the most energetic photons are emitted at smallest angles. In the right panel of Figure 5 we present the photon energy distributions for three angular upper cut-offs: 0.25, 0.5, and 1 mrad. It shows that the emitted photon energy can be selected by applying simple angular collimators.

V. CONCLUSIONS

We have evaluated and summarized the available literature data on spectroscopic properties of partially stripped ions (Li-like Pb, H-like Pb, He-like Ca and Li-like Ca) considered for the Gamma Factory project. We have demonstrated that lifetimes of relevant excited levels of these ions are accurate to a percent level or better, while corresponding transition energies reach between four and six digit accuracy. These numbers and their accuracies propagate into various parameters that will be necessary in experimental investigations.

Next, we have investigated light-ion interactions in the context of optical pumping, identifying two regimes determined by spectral properties of the ions in the bunch, i.e. the transition linewidth and the Doppler broadening. We have shown that in the case of the Doppler broadening significantly exceeding the natural linewidth of the transition, efficient pumping needs to be based on the Rabi oscillation and an appropriate tuning of light as well as a precise choice of the pulse total energy and length. We have demonstrated that under optimized conditions as much as 70% of the atoms can be excited. We have also shown that in the case of the extremely short lifetimes of the excited state, the atom can undergo multiple pumping-excitation cycles, significantly increasing the number of photons emitted from the bunch. By investigating three ions of interest (Li-like $^{208}_{82}\text{Pb}^{79+}$, Li-like $^{40}_{20}\text{Ca}^{17+}$ and H-like $^{208}_{82}\text{Pb}^{81+}$), we have identified the parameters optimizing the optical pumping and estimated the number of photons scattered by the PSI bunches.

Finally, we have described Monte Carlo simulations considering the process of the optical pumping of the H-like $^{208}_{82}\text{Pb}^{81+}$ ion in a more realistic scenario. For the simulations, we have developed the computer code GF-CAIN which is currently limited to the steady-state regime, where the classical cross-section formulation can be applied. Some exemplary results for the Gamma Fac-

TABLE VI. Some parameters for the GF-CAIN simulations and the number of spontaneously emitted photons.

PSI beam	$^{208}_{82}\text{Pb}^{81+}$
PSI mass m	$193.687 \text{ GeV}/c^2$
PSI mean energy \mathcal{E}	578.9 TeV
Beta function at the interaction point $\beta_x = \beta_y$	0.5 m
Geometric emittance $\epsilon_x = \epsilon_y$	$3 \times 10^{-9} \text{ m} \times \text{rad}$
Laser (LAB frame)	FEL (Gaussian)
Central wavelength of the laser in LAB frame λ_0^{LAB}	98.46 nm
Rayleigh length $R_{L,x} = R_{L,y}$	7.5 cm
Interaction angle ψ	0°
Atomic transition	$1s \rightarrow 2p_{1/2}$
On-resonance absorption cross section σ_0	431.7 kb
Angular distribution of emitted photons in the IRF $d^2p_1/(d\cos\theta_1 d\phi_1)$	$1/(4\pi)$
Maximum emitted photon energy in LAB frame $\hbar\omega_{\gamma}^{\text{max}}$	450 MeV
Number of emitted photons per bunch N_{γ}	2.3×10^8

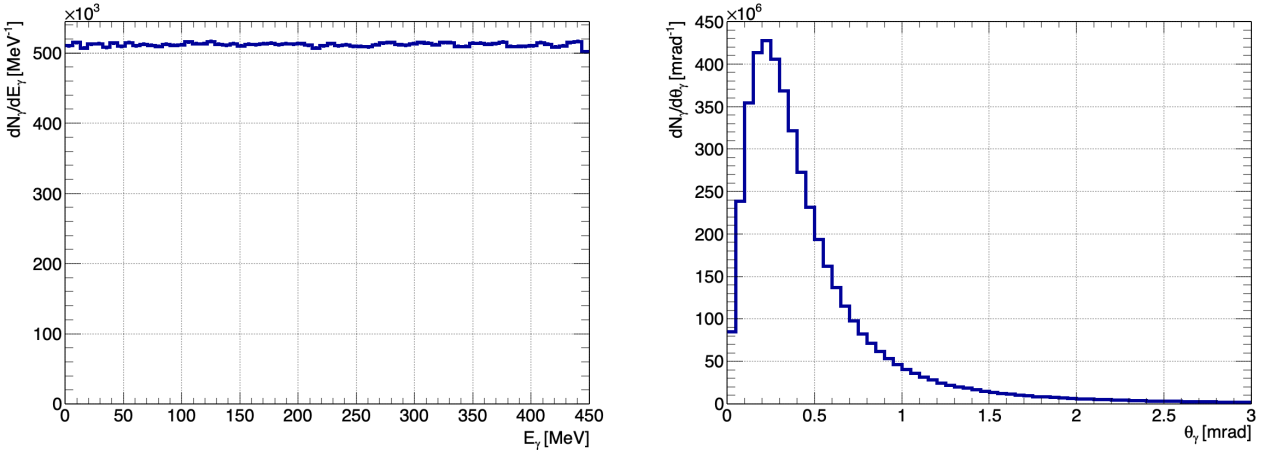


FIG. 4. Distributions of energy (left) and polar angle (right) of the spontaneously emitted photons from the H-like Pb bunch in the GF.

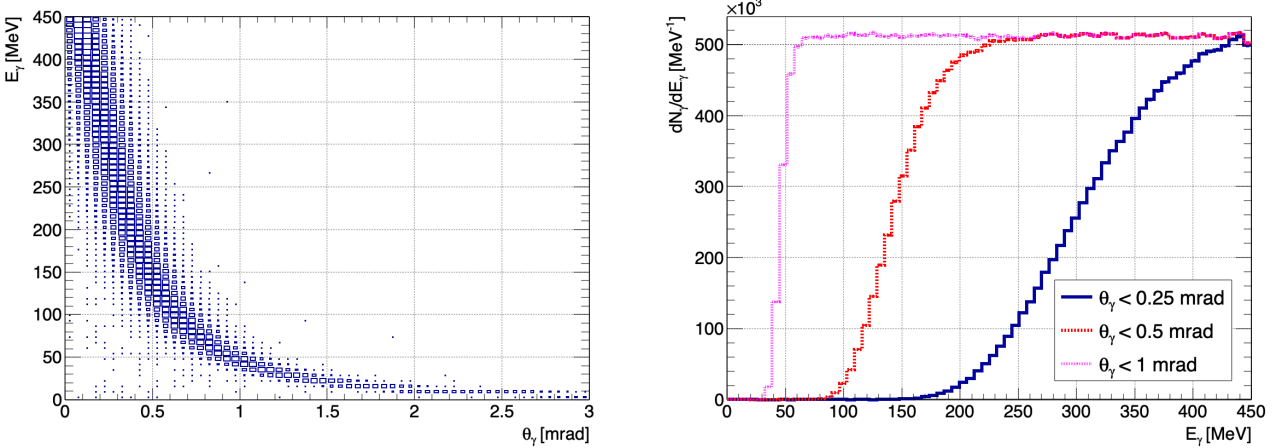


FIG. 5. Distributions of energy versus polar angle (left) and energy for three angular collimators of the spontaneously emitted photons from the H-like Pb bunch in the GF.

tory realization at the LHC with the H-like Pb-ion beam have been presented. The number of emitted photons agrees within a factor of 5 with semi-analytical calculations performed in the optical pumping formalism. In our opinion, this agreement is satisfactory given the approximations employed in the latter calculations.

The presented results form the solid ground for experimental activities associated with the optical pumping of partially stripped ions in the Gamma Factory. On the one hand, optical excitations of highly-charged heavy ions will allow to test theoretical calculations, providing access to such fundamental investigations as tests of quantum electrodynamics or violations of discrete symmetries [51], but also offering means of spin polarization of PSI and studies of collisions of such ions. On the other hand, the emission of secondary photons from the ions of

fers schemes for generation of extremely energetic (up to hundreds of MeV) and highly luminous “light” beams. Due to their unique properties, such beams when extracted from production zones and collided with external targets can be used to produce high-intensity polarized electron, positron and muon beams, high-purity neutrino beams as well as high-flux neutron and radioactive-ion beams [52].

Acknowledgements

SP acknowledges invaluable help and stimulating discussions with Dmitry Budker, Krzysztof Dzierżęga, Alexey Petrenko and Simon Rochester. JB would like to thank Andrey Surzhykov for extensive help in researching and computing spectroscopic data necessary for the Gamma Factory project. WP acknowledges the fruitful collaboration with Camilla Curatolo and Alexey Petrenko.

[1] M. W. Krasny, “*The Gamma Factory proposal for CERN*,” (2015), arXiv:1511.07794[hep-ex], arXiv:1511.07794 [hep-ex].

[2] M. W. Krasny and *et al.* (Gamma Factory Study Group) (Gamma Factory Study Group), “*Gamma Factory Proof-of-Principle experiment*,” (2019), letter-of-Intent (LoI), CERN-SPSC-2019-031, SPSC-I-253.

[3] E. G. Bessonov and K. J. Kim, Conf. Proc. C **950501**, 2895 (1996).

[4] D. Nichita, D. Balabanski, P. Constantin, M. W. Krasny, and W. Placzek, “*Radioactive ion beam production at the Gamma Factory*,” (2021), submitted to *Ann. Phys.*; arXiv:2105.13058[nucl-ex], arXiv:2105.13058 [nucl-ex].

[5] M. W. Krasny, A. Petrenko, and W. Placzek, Prog. Part. Nucl. Phys. **114**, 103792 (2020), arXiv:2003.11407 [physics.acc-ph].

[6] <https://compas.github.io>.

[7] P. Jönsson, G. Gaigalas, J. Bieroń, C. Froese Fischer, and I. P. Grant, Comput. Phys. Commun. **184**, 2197 (2013).

[8] C. Froese Fischer, G. Gaigalas, P. Jönsson, and J. Bieroń, Comput. Phys. Commun. **237**, 184 (2019).

[9] I. P. Grant, *Relativistic Quantum Theory of Atoms and Molecules: Theory and Computation* (Springer, New York, 2007).

[10] I. P. Grant, Comput. Phys. Commun. **84**, 59 (1994).

[11] K. G. Dyall, I. P. Grant, C. T. Johnson, F. A. Parpia, and E. P. Plummer, Comput. Phys. Commun. **55**, 425 (1989).

[12] B. J. McKenzie, I. P. Grant, and P. H. Norrington, Comput. Phys. Commun. **21**, 233 (1980).

[13] J. Bieroń, C. Froese Fischer, P. Indelicato, P. Jönsson, and P. Pyykkö, Phys. Rev. A **79**, 052502 (2009).

[14] J. Bieroń, C. Froese Fischer, S. Fritzsche, G. Gaigalas, I. P. Grant, P. Indelicato, P. Jönsson, and P. Pyykkö, Phys. Scr. **90**, 054011 (2015).

[15] A. Kramida, Yu. Ralchenko, J. Reader, and NIST ASD Team,.

[16] W. Johnson, Z. Liu, and J. Sapirstein, Atomic Data and Nuclear Data Tables **64**, 279 (1996).

[17] V. A. Yerokhin and A. Surzhykov, Journal of Physical and Chemical Reference Data **47**, 023105 (2018), <https://doi.org/10.1063/1.503574>.

[18] V. A. Yerokhin and A. Surzhykov, <https://aip.scitation.org/doi/10.1063/1.5034574> (2018), supplementary material to ref [17].

[19] P. Indelicato and J. Desclaux, Physical Review A **42**, 5139 (1990).

[20] Y.-K. Kim, D. Baik, P. Indelicato, and J. Desclaux, Physical Review A **44**, 148 (1991).

[21] M. H. Chen *et al.*, Phys. Rev. A **52**, 266 (1995).

[22] X. Zhang *et al.*, Phys. Rev. A **78**, 032504 (2008).

[23] Y. S. Kozhedub *et al.*, Phys. Rev. A **81**, 042513 (2010).

[24] J. Sapirstein and K. T. Cheng, Phys. Rev. A **83**, 012504 (2011).

[25] J. Sapirstein and K. T. Cheng, private communication (2019), private communication.

[26] W. R. Johnson and G. Soff, At. Data Nucl. Data Tables **33**, 405 (1985).

[27] T. Beier, P. Mohr, H. Persson, G. Plunien, M. Greiner, and G. Soff, Phys. Lett. **236**, 329 (1997).

[28] O. Jitrik and C. F. Bunge, <https://www.fisica.unam.mx/research/tables/spectra/1el/index.shtml> (2003), atomic transition probabilities for Hydrogen-like atoms.

[29] V. A. Yerokhin and V. M. Shabaev, Journal of Physical and Chemical Reference Data **44**, 033103 (2015).

[30] physics.nist.gov/cuu/Constants/index.html.

[31] A. N. Artemyev, V. M. Shabaev, V. A. Yerokhin, G. Plunien, , and G. Soff, Phys. Rev. A **71**, 062104 (2005).

[32] C. D. Lin, W. R. Johnson, and A. Dalgarno, Phys. Rev. A **15**, 154 (1977).

[33] K. M. Aggarwal and F. P. Keenan, Phys. Scr. **85**, 025306 (2021).

[34] G. W. F. Drake, Can. J. Phys. **66**, 586 (1988).

[35] J. Sapirstein and K. T. Cheng, Phys. Rev. A **83**, 012504 (2011).

[36] C. Z. Banglin Deng, Gang Jiang, Atomic Data and Nuclear Data Tables **100**, 1337 (2014).

[37] S. Nahar, Astronom. Astrophys. **389**, 716 (2002).

[38] L. J. C. Constantine E. Theodosiou, Mohammed El-Mekki, Phys. Rev. A **44**, 7144 (1991).

[39] J. Sugar and C. Corliss, *J. Phys. Chem. Ref. Data* **14** (1985), suppl. No. 2.

[40] B. Edlén, *Phys. Scr.* **28**, 51 (1983).

[41] M. Auzinsh, D. Budker, S. Rochester., *Optically Polarized Atoms: Understanding light-atom interactions* (Oxford University Press, New York, 2010).

[42] H. C. van de Hulst, *Light scattering by small particles* (Dover Publications, Inc., 2021).

[43] V. S. Letokhov and V. P. Chebotayev, *Nonlinear Laser Spectroscopy* (Springer-Verlag Berlin Heidelber GmbH, 1977).

[44] E. G. Bessonov and K. J. Kim, *Phys. Rev. Lett.* **76**, 431 (1996).

[45] P. Sprangle, A. Ting, E. Esarey, and A. Fisher, *J. Appl. Phys.* **72**, 5032 (1992).

[46] W. Płaczek, “GF-CAIN,” (2018), code available from the author: wieslaw.placzek@uj.edu.pl.

[47] K. Yokoya, “CAIN,” (2011).

[48] “International Linear Collider (ILC),” .

[49] G. S. Fishman, *Monte Carlo. Concepts, Algorithms, and Applications* (Springer, New York, 1996).

[50] C. Curatolo *et al.*, in *Proceedings, 9th International Particle Accelerator Conference (IPAC 2018): Vancouver, BC Canada* (2018) p. THPMF076.

[51] D. Budker, J. R. C. Lopez-Urrutia, A. Derevianko, V. V. Flambaum, M. W. Krasny, A. Petrenko, S. Pustelnik, A. Surzhykov, V. A. Yerokhin, and M. Zolotorev, *Ann. Phys.* **532**, 2020020204 (2020).

[52] W. Placzek *et al.*, *25th Cracow Epiphany Conference on Advances in Heavy Ion Physics (Epiphany 2019) Cracow, Poland, January 8-11, 2019*, *Acta Phys. Pol. B* **50**, 1191 (2019), arXiv:1903.09032 [physics.acc-ph].